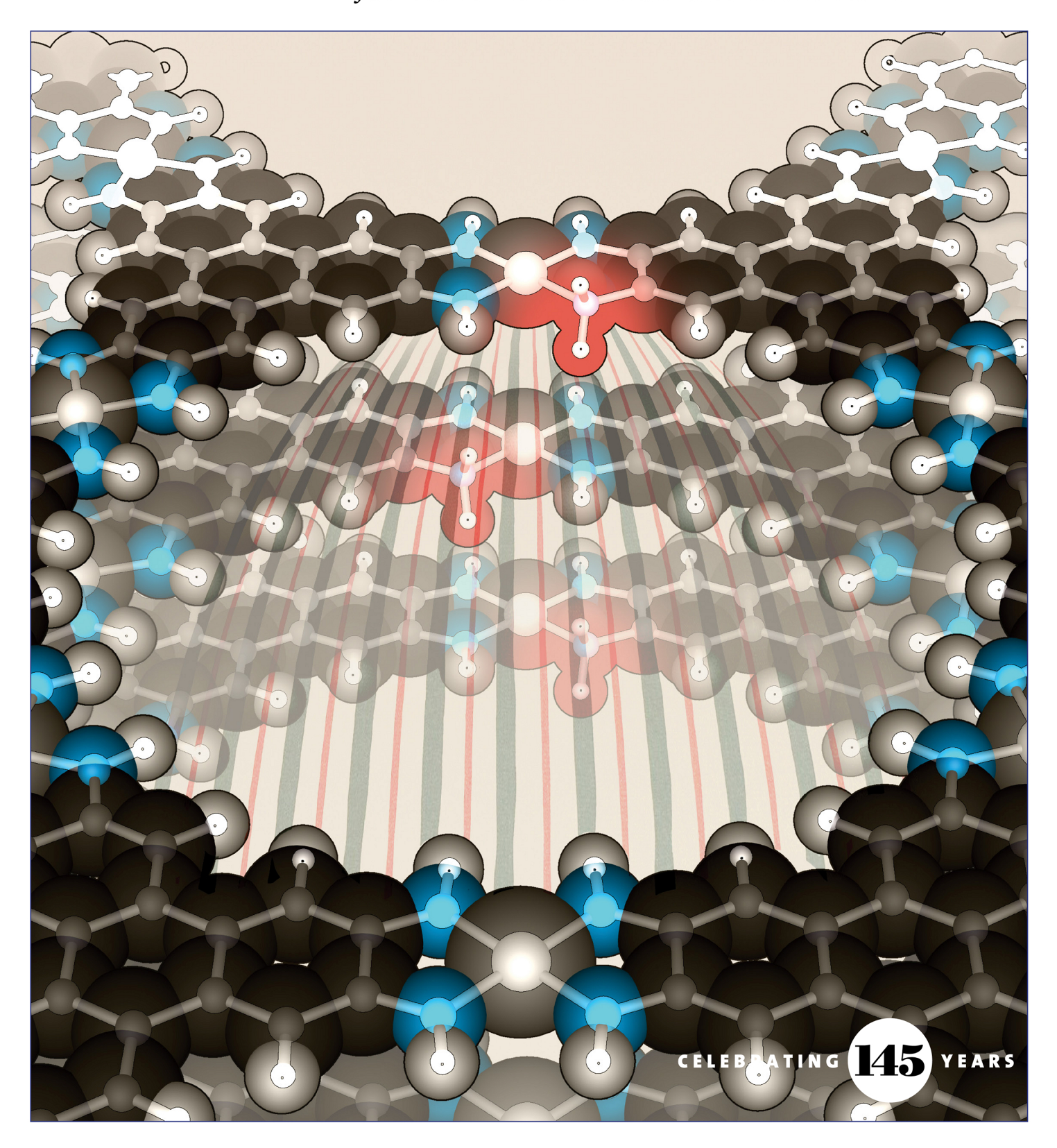
May 24, 2023
Volume 145
Number 20
pubs.acs.org/JACS

JOURNAL OF THE AMERICAN CHEMICAL SOCIETY







pubs.acs.org/JACS Article

Ligand-Mediated Hydrogenic Defects in Two-Dimensional Electrically Conductive Metal—Organic Frameworks

Tekalign T. Debela, Min Chieh Yang, and Christopher H. Hendon*



Cite This: https://doi.org/10.1021/jacs.3c02741



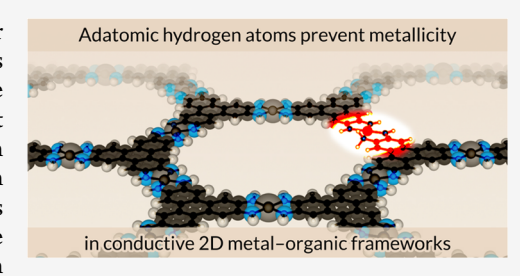
ACCESS I

III Metrics & More

Article Recommendations

s Supporting Information

ABSTRACT: Compared to dense analogues, high-surface-area metals offer several key advantages in electrocatalysis and energy storage. Of the porous manifolds, metal—organic frameworks (MOFs) boast the highest known surface area of any material class, and a subset of known frameworks also conduct electricity. The premier conductive scaffolds, Ni₃(HITP)₂ and Ni₃(HIB)₂, are both predicted to be metallic, but experiments have yet to measure bulk metallicity. In this paper, we explore the thermodynamics of hydrogen vacancies and interstitials and demonstrate that interstitial hydrogen is a plausible and prevalent defect in the conductive MOF family. The existence of this defect is predicted to render both



 $Ni_3(HITP)_2$ and $Ni_3(HIB)_2$ as bulk semiconductors, not metals, and emphasizes that hydrogenic defects play a critical role in determining the bulk properties of conductive MOFs.

INTRODUCTION

Most metal-organic frameworks (MOFs) are composed of closed-shell organic linkers and are electrical insulators. However, there is a subset of electrically conducting scaffolds that show promise for applications in energy storage technologies, 1-3 as sensors, 4 ⁻⁷ and in electrocatalysis.⁸⁻ The most conductive examples are two-dimensional (2D)connected (van der Waals (vdW)-stacked) and are generally thought to conduct in the out-of-plane direction (i.e., delocalizing charge through the intramolecular π -stack). Effort has been invested in designing MOF conductors with "through-space" or "through-bond" charge carrying pathways, 17,12 but the isolation of ordered 2D vdW single crystals is evasive. 13-18 The charge carrier identity and concentrations are also generally not known for the 2D conductive MOFs, and the sample-to-sample variability in electrical resistivity may be due to low carrier density, structural defects, or other types of chemical imperfections.

In pressed-pellet samples, grain boundaries can give rise to insulating internal interfaces. ¹⁹ It is common to see signatures of semiconducting behavior (i.e., thermally activated transport), ^{20–22} attributed to intergranular charge hopping, even for materials with computationally predicted electronic metallicity in a vdW-ordered structure. But there are other mechanisms which could lead to the signature of activated transport, including defects and misassigned structure/composition, among others. ^{23,24} Here, we study one of the more inconspicuous defects, those of adatomic and vacant hydrogen, and show that their occurrence is both thermodynamically favorable and yields semiconducting frameworks.

The champion 2D-connected conductive MOFs are constructed from hexasubstituted aromatics, two of which are shown in Figure 1a. Both $Ni_3(HITP)_2$ (HITP \equiv

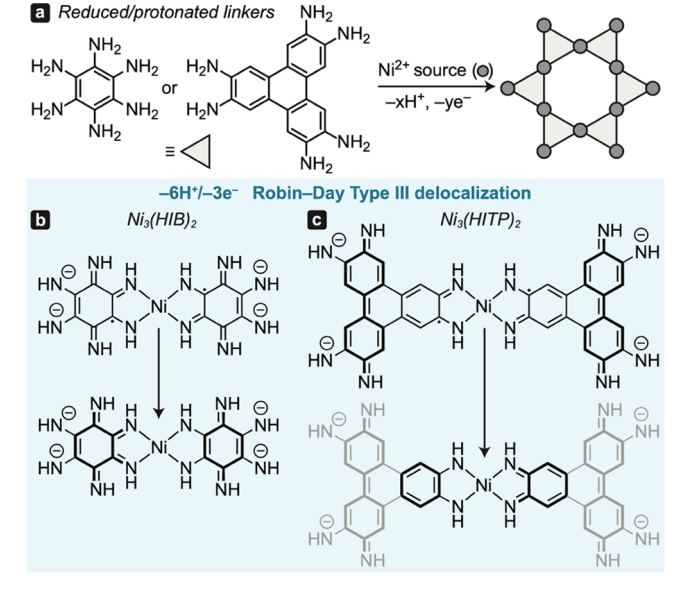


Figure 1. (a) Geometric and electronic assembly of 2D Ni₃(HIB)₂ and Ni₃(HITP)₂ requires both linker deprotonation and oxidation to form the charge-neutral kagome lattice. Resonance structures can be drawn for both (b) Ni₃(HIB)₂ and (c) Ni₃(HITP)₂, and both can be thought of as Robin–Day type III mixed valent systems.

Received: March 15, 2023

2,3,6,7,10,11-hexaiminotriphenylene)²⁵ and Ni₃(HIB)₂ (HIB \equiv hexaiminobenzene)²¹ are thought to form charge-neutral kagome lattices, accessed through a cascade of linker deprotonation and oxidation during self-assembly ($-6H^+$ and $-3e^-$ per ligand as shown in Figure 1b,c). The prenucleation oxidation and deprotonation pathways are complex (Figure S1) and offer insight into the process in which $C_6N_6H_6^{3-}$ (HIB³⁻) and $C_{18}N_6H_{12}^{3-}$ (HITP³⁻) may be obtained.

In vdW stacking configurations that yield open pores, bulk $Ni_3(HITP)_2$ is predicted to be a through-space (π -stacking) metal and in-plane semiconductor, while Ni₃(HIB)₂ is a through-bond (covalent) metal and out-of-plane semiconductor. Neither have been isolated and characterized by singlecrystal X-ray diffraction, but many of the material properties can be gleaned from predictions made from a single monolayer. As the linker is both oxidized and deprotonated, there are obvious opportunities for both protonic and electronic defect formation, i.e., if the linker was neither oxidized nor deprotonated to the extent originally assumed (yielding interstitial hydrogen, H_i) or it was over-deprotonated and oxidized (yielding a vacancy, V_H). Such defects are difficult to observe experimentally as their concentration may be low, and their spectroscopic signature may overlap with other bulk features. But there are some examples of well-characterized Hdefects in ZnO,²⁶ TiO₂,²⁷ and Pd,²⁸ among others. Here, we focus our effort to understanding the impact of vacancy and interstitial hydrogenic defects in Ni₃(HITP)₂ and Ni₃(HIB)₂.

■ RESULTS AND DISCUSSION

In the 3– oxidation state (i.e., the form that achieves high symmetry and charge neutrality in the MOF), the linkers are often drawn with three radicals or as a delocalized doublet, per the blue panel of Figure 1. Two neighboring 3– linkers can be thought of as the Robin–Day type III mixed valent, ²⁹ in effect a 4–/2– pair. The type III classification is supported by density functional theory (DFT) calculations. A calculation of a free HITP linker in the 4– and 2– charge states is predicted to be approximately 3.5 kcal/mol less stable than two 3–doublet linkers (see Figure S2), within the thermal limit of interconversion. The manifestation of this energetic preference is revealed in the electronic band structure of the periodically repeating monolayer Ni₃(HITP)₂ (Figure 2a), where it is predicted to be a narrow-gap semiconductor ($E_g = 0.21 \text{ eV}$)

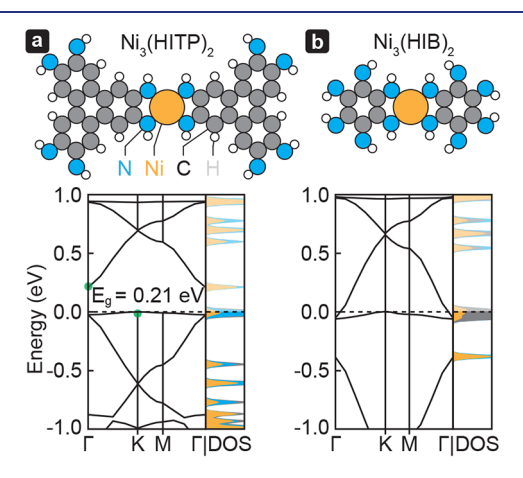


Figure 2. In-plane electronic band structure of monolayers (a) $Ni_3(HITP)_2$ and (b) $Ni_3(HIB)_2$. Γ , K, and M correspond to k-vectors of [0, 0, 0], [1/3, 1/3, 0], and [1/2, 0, 0], respectively.

rather than a metal. Conversely, HIB does not feature an extended C π -system. The addition or removal of an electron moves the entire π -system either to the *para*-imine (4–) or to a highly unstable 2– anion. As a result, the HIB-based material is predicted to behave as a monolayer metal (Figure 2, two degenerate bands at Γ , diverging at K and M) attributed to the energetic propensity to disfavor the 2– form.

Beginning with Ni₃(HIB)₂, we first examined the formation energies of hydrogenic defects in reasonable charge states, q = -1, $0(\bullet)$, and +1 (Figure 3, see the Supporting Information for

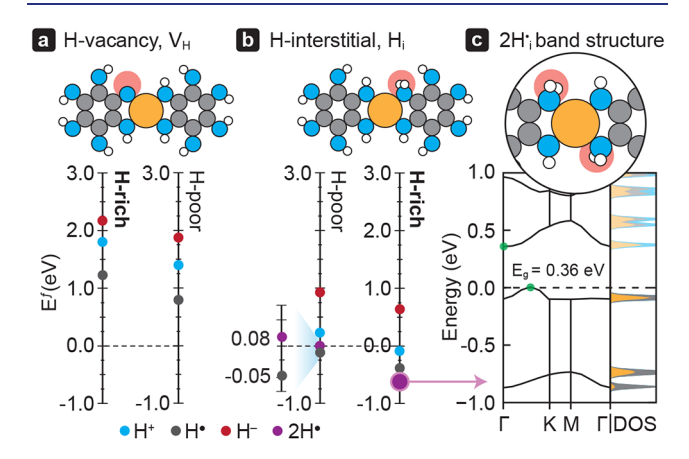


Figure 3. Defect formation energies for hydrogenic defects in $Ni_3(HIB)_2$. (a) Hydrogen vacancy and (b) interstitials in different charge states reveal that interstitial hydrogen is predicted to spontaneously form as H^+ and H^{\bullet} . The addition of a second H^{\bullet} , i.e., $2H^{\bullet}$, is the most favorable of all, as they push both linkers toward the *para*-imine form and away from Robin–Day type III delocalization. (c) The resultant electronic band structure shows the emergence of a 0.36 eV electronic band gap in monolayer $Ni_3(HIB)_2H_2$. Other hydrogenic configurations are presented in the Supporting Information and show a similar emergence of a band gap.

computational details).³⁰ Since the 2D material is a metal, the formation energy does not depend on $E_{\rm F}$ and should only depend on the charge of the defect and its location within the crystal. Since all hydrogens are equivalent, $V_{\rm H}$ are trivially defined. The position of $H_{\rm i}$, on the other hand, requires some chemical intuition—the proton will tend to localize on the most Lewis basic portion of the framework. In charge states q=0 and -1, it is difficult to predict the extent of delocalization because the addition of an electron affects the bond order of the linker, which in turn affects which atoms will partake in distribution of the charge.

We see that, in both H-rich ($\mu=H_2$) and H-poor ($\mu=C_6N_6H_{12}$, HIB) conditions (Figure S3), charge-neutral V_H (Figure 3a) are expected to form at ~0.9 eV, an energy comparable to the H_i in ZnO.³¹ In the case of H_i (Figure 3b), charge-neural adatoms are most favorable, with negative formation enthalpies. Surprisingly, the addition of a second neutral interstitial, i.e., $2H_{i\nu}$ was found to be even more negative, most pronounced in H-rich potentials (highlighted purple data point in Figure 3b). One interpretation of this result is that those defects are expected to form spontaneously or rather that the linker was likely neither oxidized nor deprotonated to the extent we had initially assumed.

Unlike conventional defects in metal oxides, the addition/removal of electrons from π -conjugated organics has a profound impact on their electronic properties. This can be

readily understood from a chemical bonding perspective. There is a thermodynamic driving force for HIB^{3-} linkers to be reduced by a single electron, pushing the linker toward the tetraanionic *para*-imine (Figure 1b) (i.e., the two-electron oxidized derivative of the aromatic starting material). If that electron is further stabilized by an adatomic H^+ , in effect a H^{\bullet} interstitial, then the system will remain charge-neutral.

2H° interstitials result in the most negative formation energies and a subsequent opening of an indirect electronic band gap of $E_g = 0.36$ eV (Figure 3c). This gap is attributed to the pairing of the radical on each linker, forming the bis-paraimine. In fact, an electronic band gap is predicted for interstitial H⁺, H⁻, H⁰, and 2H⁰ (Figure S4). This is a nice example of competing chemical effects only afforded to molecular materials. The addition of a single proton and electron into a computation that contains two linkers results in symmetry breaking, forcing the system into mixed valency. Similarly, the addition of a H- has the same effect but also shifts the Fermi level by an integer number of electrons per linker. The addition of a single H*, however, serves to pair up electrons on one linker while breaking geometric symmetry, thus resulting in a single unpaired electron on the other linker (inevitably shared between the two linkers). This is reflected in the electron band structures for these alternate configurations in Figure S4—a band gap emerges with the addition of H⁺, H[•], H-, and 2H+, and provides an alternate explanation for the characteristic activated transport in Ni₃(HIB)₂.²¹

Additionally, we note that there are 36 unique configurations in which 2H[•] can be introduced to two linkers, one example is shown in the inset of Figure 3c. We computed several configurations and concluded that they would all be in energetic competition with one another (Figure S4b). As a result, the adatomic protons are not expected to be crystallographically ordered.

Defects that introduce stoichiometric electrons per linker promote electronic restructuring in the C–C π -system. In the case of HIB, addition of single electrons promotes "reconjugation" (Figure 4a), which is certainly favored over

Figure 4. Single-electron addition per linker promotes (a) reconjugation in HIB, and (b) rearomatization in HITP.

the free radical. However, the addition of a single electron per HITP linker "rearomatizes" one arm of the triphenylene core (Figure 4b). Thus, hydrogenic defects in HITP-based materials should also be highly favorable.

To probe this hypothesis, we next turn to computing hydrogenic defect formation energies in $Ni_3(HITP)_2$. In both H-rich and -poor conditions (Figure 5a,b), V_H are predicted to form in the charge-neutral form at all E_F , at ~2.1 and ~1.8 eV,

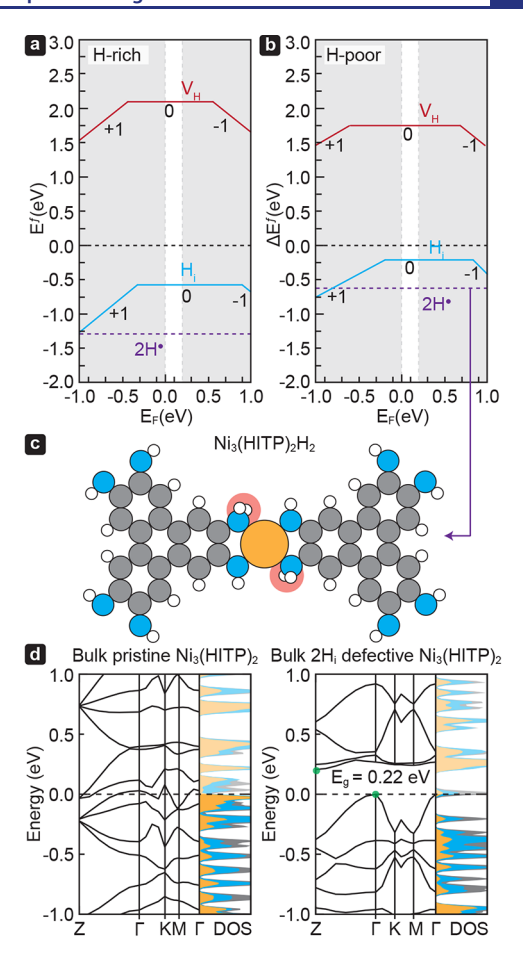


Figure 5. Defect formation energies in Ni₃(HITP)₂. (a) H-rich and (b) H-poor defect formation energy plots for hydrogenic vacancies and interstitials in charge states (q = -1, 0, +1) and the $2H^{\bullet}$ interstitial in the monolayer. One configuration of the latter is shown in (c). The electronic implication of the adatomic hydrogen results in (d) the opening of an electronic gap in both the in- and out-of-plane crystallographic directions in the bulk vdW stacked crystal.

respectively. The charge transitions occur deep within the valence and conduction bands. Like $\mathrm{Ni_3(HIB)_2}$, $\mathrm{H_i}$ are predicted to spontaneously form with negative formation energies in both H-rich and -poor potentials. Similar to $\mathrm{V_H}$, the charge transition levels occur deep within the frontier bands.

The addition of 2H• is even more favorable and, like HIB, can form in 36 unique configurations per formula unit. We sampled a few configurations, one of which is shown in Figure 5c, and others are presented in Figure S5. Energetic comparison suggests that adatomic protons are likely randomly distributed and occur in concentrations approaching one per linker. The defect formation energies were found to be between -0.5 and -1.3 eV, depending on the chemical potential. Additionally, the computed electronic band structure of monolayer Ni₃(HITP)₂ maintains a narrow electronic band gap at all computed charge states (i.e., H+, H-, H•, and 2H•, see Figure S5). Like HIB, a single adatomic hydrogen also yields a semiconducting material with spin-splitting, emphasizing the thermodynamic propensity for the triphenylene linker to rearomatize.

HITP-based materials are predicted to be "through-space" electrical conductors. Thus, to determine the impact of H[•], we must also compute the electronic band structure of 2D-stacked Ni₃(HITP)₂H₂ (i.e., the MOF featuring adatomic H[•] per

linker). Figure 5d shows the bulk electronic band structures of the pristine and stoichiometric H^{\bullet} -reduced MOF (the structure shown in Figure 5c). Here, we can see that a discrete electronic band gap is observed in both the in-plane $(\Gamma\text{-K-M-}\Gamma)$ and out-of-plane (Z-to- Γ) vectors, suggesting that the adatomic protons and electrons could be responsible for the general observation of activated electrical transport in this family of 2D conductors. This is supported by our band structure calculation, which shows that the Ni₃(HITP)₂H₂ is predicted to have an electronic band gap (0.22 eV, Figure 5d).

Finally, as with all defects, the challenge of observing these imperfections remains at large. Perhaps one could design an NMR experiment to probe the dissimilar chemical environments afforded by $-\mathrm{NH}_2$ protons. Vibrational spectroscopy offers another alternative, where the IR stretching modes of $-\mathrm{NH}$ and $-\mathrm{NH}_2$ protons are predicted to be markedly different (the former predicted to appear at $\sim\!3460-3480$ cm $^{-1}$, the latter at 3340-3400 cm $^{-1}$ see Tables S1 and S2). Such defects may prove to be more readily detected in other analogous materials (e.g., O- and S-substituted analogues), and adatomic hydrogen should have similar impact on their electronic structure.

CONCLUSIONS

In sum, this study highlights several unexplored and general aspects of defect chemistry in MOFs. First, unlike other condensed phase materials, molecular materials—in particular, those with extended $C-\pi$ systems—have numerous stable redox configurations. This makes them unique hosts for Hatom defects. For example, installing two H vacancies in hydroquinone results in the stable molecule para-benzoquinone. Should the latter be considered a defective form of its aromatic ancestor or rather a completely different material? In the case of the catechol-adjacent MOFs, like Ni₃(HITP)₂ and both S- and O-substituted analogues, the challenge is further complicated as features an extended π -manifold. The more π bonding configurations available, the more minima exist on the potential energy surface. The latter presents a conundrum in conductive MOF development because large ring systems are more stable but also offer more electronic minima (traps)³² and are hence less predictably dopable. Perhaps this offers one explanation as to why lower symmetry linkers—either aliphatic or planar linkers with π -electrons, ^{33,34} but not fully conjugated aromatics—prove to yield more electronically delocalized frameworks. At minimum, our results suggest that hydrogen defects play an operative role in determining the bulk electronic properties of the 2D conductive MOF family. They also point to a tantalizing opportunity for H-atom defect engineering, as exposure to H2 gas, or by exposing MOFs to Hatom scavengers, should allow MOF structures to equilibrate, offering unparalleled ability to tune defect concentrations postsynthetically.

ASSOCIATED CONTENT

Supporting Information

The Supporting Information is available free of charge at https://pubs.acs.org/doi/10.1021/jacs.3c02741.

Molecular and solid-state computational details and defect chemical potentials used, pKa; redox potential calculations of the HIB linker; and electronic band structures sampling other protonic orientations (PDF)

AUTHOR INFORMATION

Corresponding Author

Christopher H. Hendon – Department of Chemistry and Biochemistry, University of Oregon, Eugene, Oregon 97403, United States; orcid.org/0000-0002-7132-768X; Email: chendon@uoregon.edu

Authors

Tekalign T. Debela – Department of Chemistry and Biochemistry, University of Oregon, Eugene, Oregon 97403, United States

Min Chieh Yang – Department of Chemistry and Biochemistry, University of Oregon, Eugene, Oregon 97403, United States

Complete contact information is available at: https://pubs.acs.org/10.1021/jacs.3c02741

Notes

The authors declare no competing financial interest.

ACKNOWLEDGMENTS

This material is based upon work supported by the National Science Foundation through the Division of Materials Research under Grant DMR-1956403 and support from the Camille and Henry Dreyfus Foundation. We are also grateful for access to the Extreme Science and Engineering Discovery Environment (XSEDE), which is supported by the National Science Foundation (ACI-1548562) and the PICS Coeus High Performance Computer, which is supported by the National Science Foundation (1624776). The paper benefited from helpful discussions with M. Dincă and J. Oppenheim.

REFERENCES

- (1) Park, J.; Lee, M.; Feng, D.; Huang, Z.; Hinckley, A. C.; Yakovenko, A.; Zou, X.; Cui, Y.; Bao, Z. Stabilization of Hexaaminobenzene in a 2D Conductive Metal—Organic Framework for High Power Sodium Storage. *J. Am. Chem. Soc.* **2018**, *140*, 10315—10323.
- (2) Sheberla, D.; Bachman, J. C.; Elias, J. S.; Sun, C.-J.; Shao-Horn, Y.; Dincă, M. Conductive MOF Electrodes for Stable Supercapacitors with High Areal Capacitance. *Nat. Mater.* **2017**, *16*, 220–224.
- (3) Zheng, S.; Li, X.; Yan, B.; Hu, Q.; Xu, Y.; Xiao, X.; Xue, H.; Pang, H. Transition-Metal (Fe, Co, Ni) Based Metal-Organic Frameworks for Electrochemical Energy Storage. *Adv. Energy Mater.* **2017**, *7*, No. 1602733.
- (4) Day, R. W.; Bediako, D. K.; Rezaee, M.; Parent, L. R.; Skorupskii, G.; Arguilla, M. Q.; Hendon, C. H.; Stassen, I.; Gianneschi, N. C.; Kim, P.; Dincă, M. Single Crystals of Electrically Conductive Two-Dimensional Metal—Organic Frameworks: Structural and Electrical Transport Properties. ACS Cent. Sci. 2019, 5, 1959—1964.
- (5) Campbell, M. G.; Liu, S. F.; Swager, T. M.; Dincă, M. Chemiresistive Sensor Arrays from Conductive 2D Metal—Organic Frameworks. J. Am. Chem. Soc. 2015, 137, 13780—13783.
- (6) Stolz, R. M.; Mahdavi-Shakib, A.; Frederick, B. G.; Mirica, K. A. Host-Guest Interactions and Redox Activity in Layered Conductive Metal-Organic Frameworks. *Chem. Mater.* **2020**, *32*, 7639–7652.
- (7) Wu, G.; Huang, J.; Zang, Y.; He, J.; Xu, G. Porous Field-Effect Transistors Based on a Semiconductive Metal—Organic Framework. *J. Am. Chem. Soc.* **2017**, *139*, 1360–1363.
- (8) Ji, Y.; Dong, H.; Liu, C.; Li, Y. Two-Dimensional π -Conjugated Metal—Organic Nanosheets as Single-Atom Catalysts for the Hydrogen Evolution Reaction. *Nanoscale* **2019**, *11*, 454–458.
- (9) Miner, E. M.; Fukushima, T.; Sheberla, D.; Sun, L.; Surendranath, Y.; Dincă, M. Electrochemical Oxygen Reduction

- Catalysed by Ni₃(Hexaiminotriphenylene)₂. Nat. Commun. 2016, 7, No. 10942.
- (10) Clough, A. J.; Yoo, J. W.; Mecklenburg, M. H.; Marinescu, S. C. Two-Dimensional Metal—Organic Surfaces for Efficient Hydrogen Evolution from Water. *J. Am. Chem. Soc.* **2015**, *137*, 118–121.
- (11) Xie, L. S.; Skorupskii, G.; Dincă, M. Electrically Conductive Metal-Organic Frameworks. *Chem. Rev.* **2020**, *120*, 8536–8580.
- (12) Meng, Z.; Jones, C. G.; Farid, S.; Khan, I. U.; Nelson, H. M.; Mirica, K. A. Unraveling the Electrical and Magnetic Properties of Layered Conductive Metal-Organic Framework With Atomic Precision. *Angew. Chem.* **2022**, *134*, No. e202113569.
- (13) Snook, K. M.; Zasada, L. B.; Chehada, D.; Xiao, D. J. Oxidative Control over the Morphology of Cu₃(HHTP)₂, a 2D Conductive Metal–Organic Framework. *Chem. Sci.* **2022**, *13*, 10472–10478.
- (14) Skorupskii, G.; Chanteux, G.; Le, K. N.; Stassen, I.; Hendon, C. H.; Dincă, M. Electrical Conductivity through $\pi-\pi$ Stacking in a Two-dimensional Porous Gallium Catecholate Metal–Organic Framework. *Ann. N. Y. Acad. Sci.* **2022**, *1518*, 226–230.
- (15) Skorupskii, G.; Le, K. N.; Cordova, D. L. M.; Yang, L.; Chen, T.; Hendon, C. H.; Arguilla, M. Q.; Dincă, M. Porous Lanthanide Metal–Organic Frameworks with Metallic Conductivity. *Proc. Natl. Acad. Sci. U.S.A.* **2022**, *119*, No. e2205127119.
- (16) Skorupskii, G.; Trump, B. A.; Kasel, T. W.; Brown, C. M.; Hendon, C. H.; Dincă, M. Efficient and Tunable One-Dimensional Charge Transport in Layered Lanthanide Metal—Organic Frameworks. *Nat. Chem.* **2020**, *12*, 131–136.
- (17) Dou, J.-H.; Arguilla, M. Q.; Luo, Y.; Li, J.; Zhang, W.; Sun, L.; Mancuso, J. L.; Yang, L.; Chen, T.; Parent, L. R.; Skorupskii, G.; Libretto, N. J.; Sun, C.; Yang, M. C.; Dip, P. V.; Brignole, E. J.; Miller, J. T.; Kong, J.; Hendon, C. H.; Sun, J.; Dincă, M. Atomically Precise Single-Crystal Structures of Electrically Conducting 2D Metal—Organic Frameworks. *Nat. Mater.* 2021, 20, 222—228.
- (18) Hmadeh, M.; Lu, Z.; Liu, Z.; Gándara, F.; Furukawa, H.; Wan, S.; Augustyn, V.; Chang, R.; Liao, L.; Zhou, F.; Perre, E.; Ozolins, V.; Suenaga, K.; Duan, X.; Dunn, B.; Yamamto, Y.; Terasaki, O.; Yaghi, O. M. New Porous Crystals of Extended Metal-Catecholates. *Chem. Mater.* **2012**, 24, 3511–3513.
- (19) Foster, M. E.; Sohlberg, K.; Allendorf, M. D.; Talin, A. A. Unraveling the Semiconducting/Metallic Discrepancy in Ni₃(HITP)₂. *J. Phys. Chem. Lett.* **2018**, *9*, 481–486.
- (20) Clough, A. J.; Skelton, J. M.; Downes, C. A.; de la Rosa, A. A.; Yoo, J. W.; Walsh, A.; Melot, B. C.; Marinescu, S. C. Metallic Conductivity in a Two-Dimensional Cobalt Dithiolene Metal—Organic Framework. *J. Am. Chem. Soc.* **2017**, *139*, 10863—10867.
- (21) Dou, J.-H.; Sun, L.; Ge, Y.; Li, W.; Hendon, C. H.; Li, J.; Gul, S.; Yano, J.; Stach, E. A.; Dincă, M. Signature of Metallic Behavior in the Metal—Organic Frameworks M₃(Hexaiminobenzene)₂ (M = Ni, Cu). *J. Am. Chem. Soc.* **2017**, *139*, 13608–13611.
- (22) Chen, T.; Dou, J.-H.; Yang, L.; Sun, C.; Libretto, N. J.; Skorupskii, G.; Miller, J. T.; Dincă, M. Continuous Electrical Conductivity Variation in M_3 (Hexaiminotriphenylene)₂ (M = Co, Ni, Cu) MOF Alloys. *J. Am. Chem. Soc.* **2020**, *142*, 12367–12373.
- (23) Foster, M. E.; Sohlberg, K.; Spataru, C. D.; Allendorf, M. D. Proposed Modification of the Graphene Analogue Ni₃(HITP)₂ To Yield a Semiconducting Material. *J. Phys. Chem. C* **2016**, *120*, 15001–15008.
- (24) Le, K. N.; Mancuso, J. L.; Hendon, C. H. Electronic Challenges of Retrofitting 2D Electrically Conductive MOFs to Form 3D Conductive Lattices. ACS Appl. Electron. Mater. 2021, 3, 2017–2023.
- (25) Sheberla, D.; Sun, L.; Blood-Forsythe, M. A.; Er, S.; Wade, C. R.; Brozek, C. K.; Aspuru-Guzik, A.; Dincă, M. High Electrical Conductivity in Ni₃(2,3,6,7,10,11-Hexaiminotriphenylene)₂, a Semiconducting Metal–Organic Graphene Analogue. *J. Am. Chem. Soc.* **2014**, *136*, 8859–8862.
- (26) McCluskey, M. D.; Jokela, S. J. Defects in ZnO. *J. Appl. Phys.* **2009**, *106*, No. 071101.
- (27) Lavrov, E. V.; Chaplygin, I.; Herklotz, F.; Melnikov, V. V.; Kutin, Y. Hydrogen in Single-Crystalline Anatase TiO₂. *J. Appl. Phys.* **2022**, *131*, No. 030902.

- (28) Oates, W. A.; Flanagan, T. B. The Reaction of Hydrogen Atoms with Palladium and Its Alloys. *Can. J. Chem.* **1975**, *53*, 694–701.
- (29) Robin, M. B.; Day, P. Mixed Valence Chemistry-A Survey and Classification. In *Advances in Inorganic Chemistry and Radiochemistry*; Elsevier, 1968; Vol. 10, pp 247–422.
- (30) Kim, S.; Hood, S. N.; Park, J.-S.; Whalley, L. D.; Walsh, A. Quick-Start Guide for First-Principles Modelling of Point Defects in Crystalline Materials. *J. Phys.: Energy* **2020**, 2, No. 036001.
- (31) Van de Walle, C. G. Hydrogen as a Cause of Doping in Zinc Oxide. *Phys. Rev. Lett.* **2000**, *85*, 1012–1015.
- (32) Demuth, M. C.; Hendon, C. H. Linker Aromaticity Reduces Band Dispersion in 2D Conductive Metal—Organic Frameworks. *ACS Mater. Lett.* **2023**, *5*, 1476—1480.
- (33) Su, X.; Zhong, Z.; Yan, X.; Zhang, T.; Wang, C.; Wang, Y.-X.; Xu, G.; Chen, L. Facile Synthesis of Metallosalphen-Based 2D Conductive Metal-Organic Frameworks for NO₂ Sensing: Metal Coordination Induced Planarization. *Angew. Chem., Int. Ed.* **2023**, No. e202302645.
- (34) Yang, Z.; Hao, W.; Su, X.; Zhang, T.; Chen, W.; Zhang, G.; Chen, L. Metallosalphen-Based 2D Covalent Organic Frameworks with an Unprecedented **Tju** Topology via K-Shaped Two-in-One Monomers. *Chem. Mater.* **2022**, *34*, 5888–5895.